CHEMISTRY
A European Journal

A Journal of
ChemPubSoc Europe

Accepted Article

Title: Self-assembly of perylenediimide-single strand DNA conjugates: Employing hydrophobic interactions and DNA base pairing to create a diverse structural space

Authors: Frederick Lewis, Ashutosh Kumar Mishra, Haim Weissman, Elisha Krieg, Kevin A. Voltaw, Martin McCullagh, and Boris Rybtchiinski

To be cited as: *Chem. Eur. J.* 10.1002/chem.201700752

Link to VoR: http://dx.doi.org/10.1002/chem.201700752

Supported by
ACES

WILEY-VCH

10.1002/chem.201700752

WILEY-VCH

Self-assembly of perylenediimide-single strand DNA conjugates: Employing hydrophobic interactions and DNA base pairing to create a diverse structural space

Ashutosh Kumar Mishra,[a] Haim Weissman,[b] Elisha Krieg,[b] Kevin A. Votaw,[c] Martin McCullagh,[c] Boris Rybtchinski,*[b] and Frederick D Lewis*[a]

Abstract: The self-assembly behaviour of DNA conjugates possessing a perylenediimide (PDI) head group and a *N*-oligonucleotide tail has been investigated using a combination of optical spectroscopy and cryogenic transmission electron microscopy (cryo-TEM) imaging. In order to obtain insight into the interplay between PDI hydrophobic interactions and DNA base pairing we employed systematic variation in the length and composition of the oligo tails. Conjugates with short $(TA)_n$ or $(CG)_n$ oligo tails ($n \leq 3$) form helical or nonhelical fibres constructed from π-stacked PDI head groups with pendent oligo tails in aqueous solution. Conjugates with longer $(TA)_n$ oligo tails also form stacks of PDI head groups, which are further aggregated by base pairing between their oligo tails, leading to fibre bundling and formation of bilayers. The longer $(CG)_n$ conjugates form PDI end-capped duplexes, which further assemble into PDI-stacked arrays of duplexes leading to large scale ordered assemblies. Cryo-TEM imaging reveals that $(CG)_3$ gives rise to both fibres and large assemblies, while $(CG)_5$ assembles preferentially into large ordered structures. Introduction

Introduction

The self-assembly of derivatives of perylenediimide (PDI) into dimers and stacked columnar aggregates has been extensively investigated both in organic solvents and in water.[1, 2, 3] Owing to the hydrophobic nature of PDI, water solubility requires the presence of hydrophilic substituents. Among the hydrophilic substituents that have been investigated are polyethers,[4] polyamines,[4, 5] peptides,[1, 6] polypeptides, oligonucleotides,[3] and dendrons having terminal carboxylate[7] or hydroxyl groups.[8]

The dimerization and oligomerization of DNA-perylenediimide (PDI) conjugates involving PDI stacking motifs has been the subject of several investigations.[3] Li and co-workers reported the hydrophobic stacking of 2 to 5 PDI chromophores connected in head-to-tail fashion in a single strand by tetraethyleneglycol linkers.[9] Wagenknecht and co-workers reported the self-assembly of 5'-PDI-modified DNA conjugates to form PDI-end capped duplexes and three way junctions and the hydrophobic association of these constructs to form linear oligomers and DNA triangles, respectively.[10, 11] Formation of inter- and intramolecular PDI dimers and oligomers upon duplex and hairpin formation[12],[13] or non-covalent binding of PDI at abasic sites[14] has also been reported. We previously reported that the PDI-DNA hairpin **H8**, which possesses a PDI linker,[15] exists as a monomer in water in the absence of salt but undergoes dimerization in the presence of 100 mM NaCl (Scheme 1a,b).[16] Similarly, the PDI-DNA dumbbell **D8** exists predominantly as a monomer in water but undergoes self-assembly into an end-to-end oligomer in the presence of added NaCl (Scheme 1c).[17, 18] Wu et al. reported that salt-induced assembly of a guanine-PDI conjugate results in the formation of G-quartets with pairs of stacked PDI units on the perimeter.[19] However, to date there have been no reports of the formation of higher-order aggregates involving interactions between columnar stacks of PDI-oligonucleotide conjugates and their DNA tails.

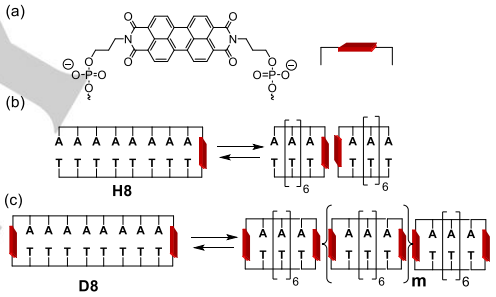

Scheme 1. Structures of (a) a PDI linker, (b) the hairpin **H8** and its head-to-head dimer, and (c) the dumbbell **D8** and its end-to-end oligomer.

We envisaged that hierarchical structures that utilize PDI aggregation together with oligonucleotide base pairing might lead to structural diversity and complexity. In order to investigate the propensities of PDI-DNA conjugates to engage in both stacking and base pairing we aimed at systematic variation of the single strand DNA (c.f.) length and composition (Chart 1). These conjugates possess a racemic *N*-alkyl PDI head group[20] and an alternating $d(TA)_n$ or $d(CG)_n$ (n = 1-5) oligonucleotide tail attached to an *N'*-hyroxypropyl linker. Herein, we report on a combined spectroscopic and structural imaging (cryo-TEM) study on the self-assembly of the conjugates in solution. All of the $(TA)_n$ conjugates and the shorter $(CG)_n$ conjugates form PDI π-stacked aggregates in water even at low concentrations. In addition, conjugates possessing four or five $(TA)_n$ repeats form PDI π-stacked aggregates that are further assembled into bundles or bilayers by nucleotide base pairing connecting the PDI molecules in different stacks. The longer $(CG)_n$ conjugates form end-capped duplexes which can further assemble into ordered PDI π-stacked arrays. Thus, the PDI-single-strand DNA conjugates can assemble into fibres having different degrees of helicity, fibre bundles, bilayer structures, and large

[a] Dr. A. K. Mishra, Prof. F. D. Lewis
Department of Chemistry, Northwestern University
Evanston, Illinois 60208-3113, USA
E-mail: fdl@northwestern.edu
[b] Dr. H. Weissman, Dr. E. Krieg, and Prof. B. Rybtchinski
Department of Organic Chemistry, Weizmann Institute of Science
Rehovot 76100, Israel
E-mail: boris.rybtchinski@weizmann.ac.il
[c] Mr. K. A. Votaw and Prof. M. McCullagh
Department of Chemistry, Colorado State University
Fort Collins, Colorado 80523, USA

Supporting information for this article is given via a link at the end of the document.

ordered arrays of stacked PDIs connected by base-paired duplexes. This unprecedented structural diversity is observed for the first time for PDI-DNA aggregates. Our study suggests guidelines regarding the interplay of base pairing and hydrophobic interactions that can be employed for the rational design of simple and complex PDI-DNA assemblies.

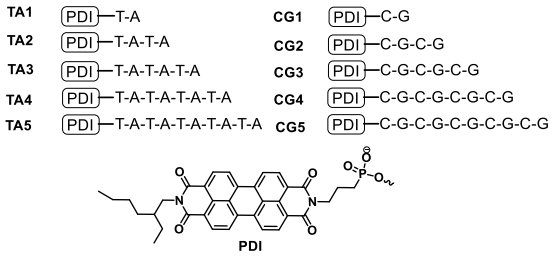

Chart 1. Structures of the **TA1-5** and **CG1-5** conjugates and the PDI head group.

Results and Discussion

Based upon differences in the cryo-TEM images and the optical spectra of the PDI-oligo conjugates **TA1-5** and **CG1-5** we will demonstrate that the combination of *N*-alkyl-PDI hydrophobic interactions and base pairing between the $(TA)_n$ and $(CG)_n$ oligo tails can result in a diverse structural space, the character of which is dependent upon both the length and base composition of the oligo tail and the external conditions (solvent, concentration, temperature, etc.). In dealing with this diversity of structures, we will begin with the conjugates possessing the shortest oligo tails. These conjugates have limited solubility in aqueous solution and form one-dimensional PDI-stacked assemblies, but do not form inter-molecular or inter-fibre hydrogen bonds. As the length of the oligo tails increases, the solubility of the conjugates increases as does the propensity to form hydrogen bonds between the oligonucleotide groups, resulting in more structural diversity. In the following sections, conjugates which form similar structural types will be discussed together, with structural information obtained from molecular modeling and cryo-TEM images being introduced prior to information drawn from solution phase optical spectroscopy.

Synthesis and Molecular Modelling. The synthesis, purification, and characterization of conjugates **TA1-5** and **CG1-5** (Chart 1) are described in the Experimental Section and in the Supporting Information (SI, Fig. S1 and Table S1). The conjugates and their structures are further characterized by molecular dynamics simulations, cryogenic transmission electron microscopy (cryo-TEM) imaging, and optical spectroscopy, as described in the main text and SI.

In order to obtain information about the likely π-stacking geometry of the PDI conjugates we have undertaken molecular dynamics simulations of homo-dimers of the two conjugates having the shortest $(TA)_n$ oligo tails, **TA1** and **TA2**. The details of the simulations, including the parameters for the PDI moiety, can be found in the Experimental Section and SI. All-atom molecular dynamics simulations were run on six different starting conformations of two **TA1** conjugates initially separated by at least 12 Å in water with only neutralizing ions present. Of the six, five resulted in PDI dimer conformations in which the TA tails are anti (most populated dihedral angles ± 145°, Fig. 1a) and one syn (dihedral angle 30°, Figure 1b, see also Scheme 2).

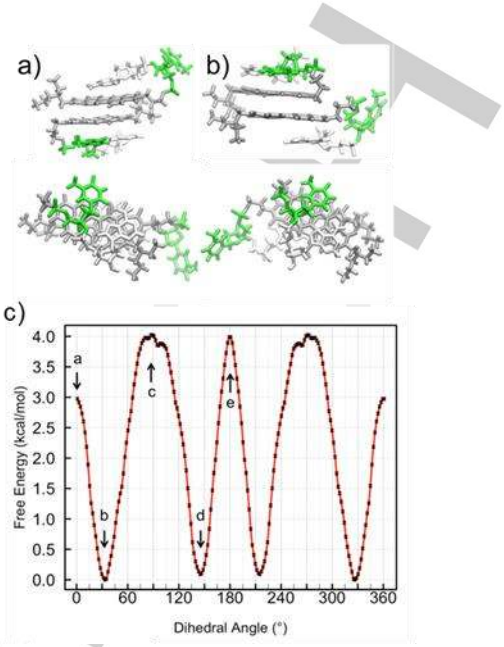

Figure 1. Side view (above) and top view (below) for (a) anti- and (b) syn-conformations for **TA1** dimers. The alkyl and nucleotide chains are pointed in the same direction along the normal to the PDI plane. (c) Potential mean force for the rotation along the dihedral angle for the PDI dimer in **TA1**. **b** and **d** are the syn- and anti-conformers, respectively, and **a**, **c**, and **e** are the barriers separating these conformers..

The probability density distributions of the PDI-PDI dihedral angles for the six dimer simulations are reported in Figure S3, SI. Four of the anti-conformations and the syn conformation have their alkyl and TA groups pointed in the same direction with respect to the PDI plane, allowing close approach of the dimer PDI π surfaces (Figure 1a). More limited molecular dynamics simulations for **TA2** showed that it formed dimer conformations similar to those for **TA1**.

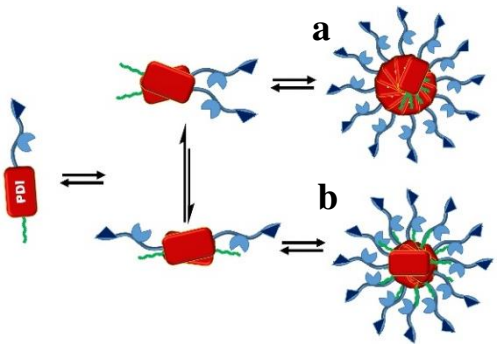

Scheme 2. Schematic dimerization of **TA1** or **CG1** (dinucleotide in blue and *N*-alkyl substituent in green) and further aggregation of the syn- and anti-dimers to form **(a)** chiral helical assembly of all-syn dimers and **(b)** achiral assembly of anti-dimers assembled in alternating ± fashion.

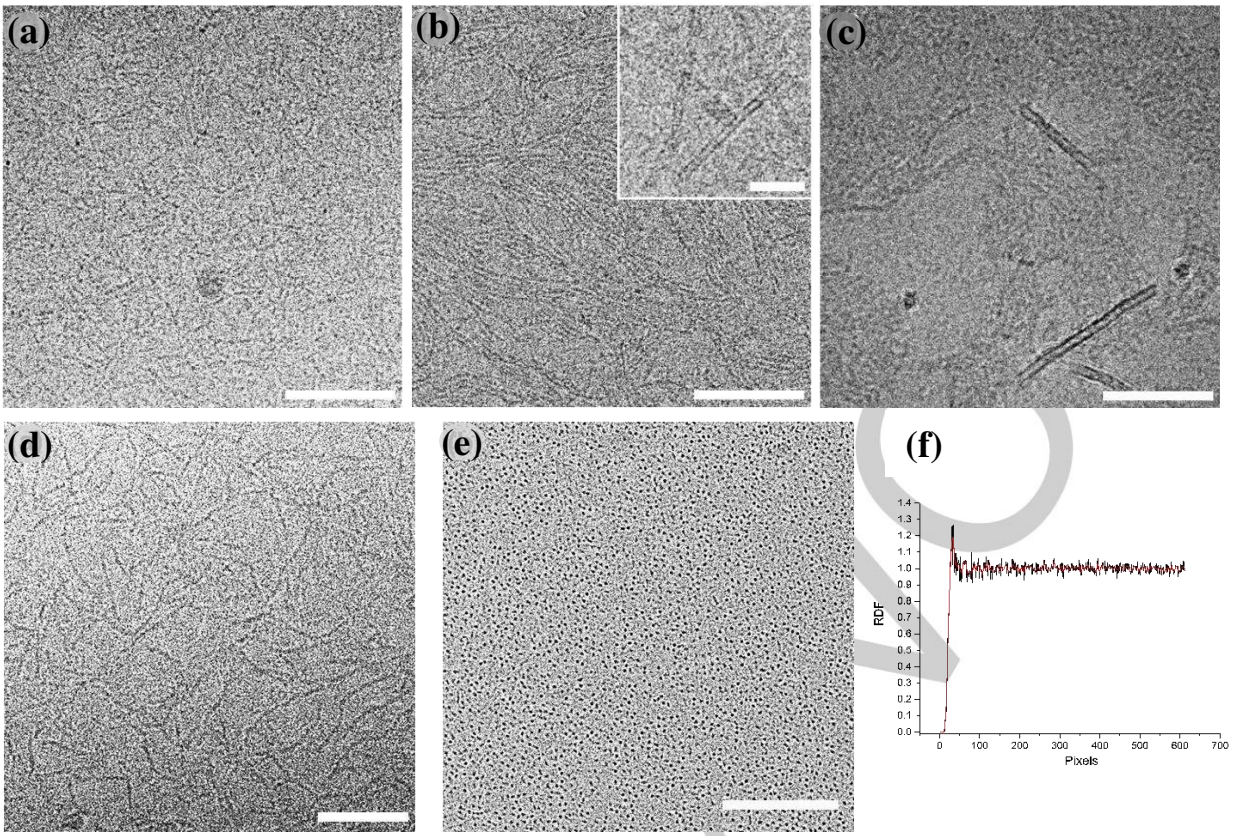

Figure 2. (upper panels) Cryo-TEM images of **TA1**, **TA4**, and **TA5**. Scale bar is 50 nm. (a) **TA1** (conc. 5.5·10-5 M in 10 mM phosphate buffer, pH 7.2) after aging 5 d at room temperature. (b) **TA4** (conc. 2.0·10-5 M in 10 mM phosphate buffer, pH 7.2) aged 26 h at room temperature. Inset: Parallel high-contrast features typical of bilayers (occasionally observed). Scale bar 25 nm. (c) **TA5** (conc. 2.0·10-5 M in 10 mM sodium phosphate buffer, pH 7.2) aged 26 h at room temperature. Parallel high-contrast features are observed in all images. (lower panels) Cryo-TEM images: (d) **CG2** (conc. 2.0·10-5 M, 10 mM phosphate buffer pH 7.2); (e) **CG5** (conc. 2.0·10-5 M, 10% THF, v/v, 10 mM phosphate buffer pH 7.2 solution) obtained after aging 27.5 h at room temperature; (f) Radial distribution function (RDF, 0.1471 nm/px) for the tips of fibres shown in (e). Red line, FFT filtration (by 2 data points) of the RDF, indicates the radius of the shortest possible contact of 1.2±0.1 nm. The highest probability for interaction, g(r)max, is observed at 5.8±0.6 nm with a secondary peak at 11.2±0.7 nm. THF was added in order to improve the quality of the cryo-TEM samples of **CG5**. Spectroscopic studies showed that THF addition (10% v) does not change significantly the appearance of the spectra.

.The hydrophobic PDI faces in all of the structures are at least partially covered by their short oligo tails (Figure 1a,b). The relative energies of the syn- and anti-conformations and the barriers for their interconversion were calculated by umbrella sampling along the PDI dimer major axis (Figure S4, SI).[22] These calculations provide the potential of mean force (PMF) for full rotation about the dimer major axis dihedral angle shown in Figure 1c for **TA1**. Surprisingly, the difference in relative free energy between the syn- and anti-conformation is only 0.10±0.06 kcal/mol, the syn conformation at slightly lower energy. The calculated barrier for interconversion of syn conformations (30° to 330° through 0°) is 3.00±0.06 kcal/mol, larger than the value of 1.0 kcal/mol reported for the dimer of unsubstituted PDI molecules in water.[16] The larger value presumably is a consequence of the presence of *N*-alkyl and dinucleotide substituents. A barrier of 3.90±0.06 kcal/mol is calculated for interconversion of syn- and anti-conformers, similar to the value calculated for the perpendicular PDI dimer. Similar results are obtained for **TA2**. In this case the anti-conformation is lower in energy by 0.15±0.06 kcal/mol and the barriers are higher than for **TA1** by 0.3-0.5 kcal/mol. Molecular dynamics simulations for trimers of **TA1** and for conjugates with longer oligo tails were not undertaken.

Structures of Conjugates TA1-3 and CG1-2. Cryo-TEM images of the conjugates in Chart 1 are shown in Figure 2 and in Figures S5-S9, SI. Samples were aged at room temperature for a minimum of 24 hr prior to imaging to assure formation of equilibrated aggregates. Further aging did not result in observable changes in the images. **TA1**, **TA2** and **TA3** (Figure 2a, S5, and S6, respectively) display formation of fibres. The width of the high contrast domains of the fibres is similar for the **TA1-3** systems (1.2±0.2, 1.3±0.2 and 1.2±0.2 nm, respectively, Table S3) as is their length (17±9, 13±5, 15±8 nm respectively; the fibre length estimation is an approximate one due to the difficulty to trace fibre termini). The observed width of the fibres in the three systems indicates a supramolecular architecture where PDI head groups (PDI core is ca. 1.2 nm) are stacked and are responsible for the observed high contrast areas, whereas the oligo tails exhibit low contrast, as expected for highly solvated groups. The crystal structure of a slipped stack of *N,N*-dipropyl-PDI has a center-to-center distance of 4.6 Å, corresponding to the π-stacking of 35 conjugates in a 16 nm fibre.[21] A 16 nm stack of conjugates with aligned centers and a plane-to-plane spacing of 3.5 Å would contain approximately 46 stacked PDI monomers.

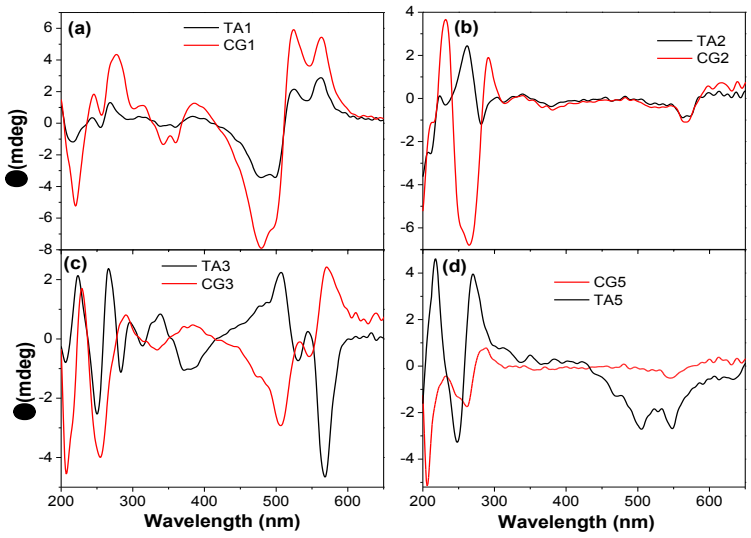

Figure 3. CD spectra of TA1-3,5 and CG1-3,5 in 10 mM phosphate buffer (pH 7.2) at room temperature. Spectra are unchanged from ca. 0.2-24 hr.

The cryo-TEM images for **CG1** (Figure S7, SI) display relatively disordered fibrous aggregates, where the fibres have a high contrast width of 1.6±0.2 nm. **CG2** molecular fibres have a higher contrast width of 2.1±0.2 nm (Figure 2a, lower row), an average length of 44±24 nm, and a maximum measured length of ca. 119 nm.

Information about the solution phase structures of these conjugates is available from their optical spectra. Their CD spectra are shown in Figure 3 and S10, SI. The long-wavelength region of the spectra of **TA1** and **CG1** (Figure 3a) display strong positive bands near 550 nm and negative bands near 480 nm, similar to those reported previously for helical aggregates of chiral PDI derivatives.[6, 7, 22] In addition to the positive Cotton effect observed at long wavelengths, weaker positive and negative bands are observed near 385 and 350 nm, respectively, assigned to the weak second PDI π,π^* transition. The CD spectrum for **TA3** (Figure 3c) is similar to those of **TA1** and **CG1**, except that the longest wavelength bands are not split and **TA3** has a negative Cotton effect for both bissignate PDI bands. The CD spectra of **TA2** and **CG2** (Figure 3b) do not display bissignate bands at long wavelength, but only weak negative bands. The temperature-dependent CD spectra of **TA3** and several other conjugates are shown in Figure S11, SI. A thermal dissociation profile for either of the long wavelength CD bands of **TA3** provides a CD melting temperature of T_M = 30 ± 1°C.

Since the PDI chromophore is achiral, we attribute the long wavelength CD bands of **TA1**, **TA3**, and **CG1** to the chiral environment of a helical stacked aggregate in which the oligo tails adopt either an all-syn conformation, in accord with the calculated energy minimum for the **TA1** dimer, or an all-anti conformation (Scheme 2a). The CD spectra of **TA2** and **CG2** display only weak negative bands corresponding to their two long-wavelength PDI absorption bands (Figure 3b). This might reflect either similar amounts of syn- and anti-stacked aggregates or achiral ± stacking of anti-dimers (Scheme 2b). The similar calculated energies for the syn- and anti-conformations of **TA1** and **TA2** provides a plausible explanation for the differences in their CD spectra. The short-wavelength regions (200-300 nm) of the CD spectra of **TA1-3** do not match that of the duplex $(TA)_5$•$TA)_5$ in aqueous buffer containing 0.1 M NaCl (Figure S12, SI). Similarly, the short-wavelength region of **CG2** does not match that of $(CG)_3$•$(CG)_3$. Thus the *N*-oligo tails of these conjugates apparently are too short to form either intermolecular or interfibre duplexes.

The concentration-dependent UV-visible spectra of the conjugates in aqueous buffer (10 mM sodium phosphate) in the absence of added salt are shown in Figure 4 and S13, SI. The long-wavelength absorption bands (> 300 nm) are assigned to the PDI chromophore, whereas the shorter wavelength bands are assigned to overlapping absorption of the nucleotides and the weak higher energy transitions of PDI.[16] The long-wavelength regions of the spectra in buffer display vibronic band maxima at ca. 505±3 nm and 543±5 nm with band intensity ratios intermediate between the values expected for PDI monomer (>1.4) and stacked dimers or aggregates (< 0.6).[3] PDI 0,1 and 0,0 vibronic band maxima and 0,0/0,1 intensity ratios for conjugates **TA1-5** and **CG1-5** at 5 °C and 90 °C in aqueous buffer are summarized in Table 1.

Table 1. PDI 0,1 and 0,0 vibronic band maxima and 0,0/0,1 intensity ratios for conjugates **TA1-5** and **CG1-5** at 5 °C and 90 °C in aqueous buffer.

Temp.	5 °C			90 °C		
λ, nm	0,1	0,0	Ratio	0,1	0,0	Ratio
TA1	503	551	0.57	499	536	0.73
TA2	506	548	0.73	501	537	1.05
TA3	506	548	0.80	500	537	1.25
TA4	503	547	0.70	498	535	0.93
TA5	504	546	0.78	498	538	0.99
CG1	503	553	0.56	499	537	0.66
CG2	507	551	0.75	503	539	0.98
CG3	507	546	0.67	503	538	1.15
CG4	508	546	0.83	504	540	1.34
CG5	506	543	0.72	502	538	1.20

The concentration dependence of the PDI vibronic band intensity ratios for the **TA1-5** and **CG1-5** are shown in Figure 5a,b. The 0,0/0,1 vibronic band intensity ratios of the long-wavelength region of the UV spectra of the conjugates **TA1** and **CG1** are independent of concentration and have low values (< 0.6) indicative of high aggregate/monomer ratios and well-stacked PDI chromophores even at low concentrations. The vibronic band intensity ratios for **TA2** and **CG2** are also relatively independent of concentration, indicative of high aggregate/monomer ratios, but have higher vibronic band intensity ratios (~ 0.75, Figure 5). The higher band intensity ratios plausibly result from slipped-stacked geometries with

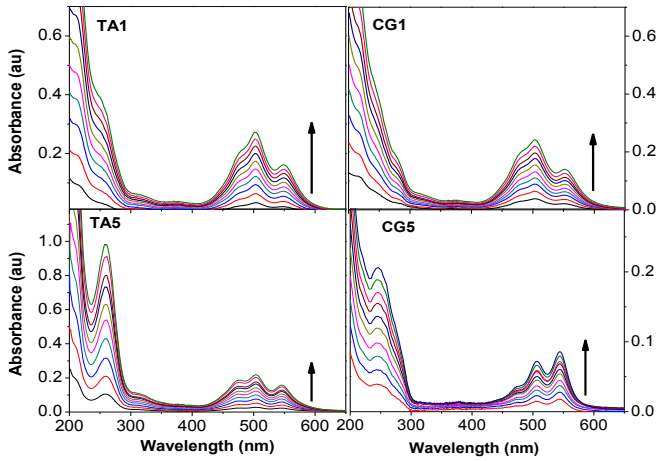

Figure 4. Concentration dependence of the UV visible spectra of **TA1**, **TA5**, **CG1** and **CG 5** in aqueous buffer (pH 7.2). Concentration range for **TA1**, **TA5**, **CG1** and **CG5** are 0.86 – 7.4, 0.74-5.9, 1.03-6.5 and 0.37-2.16 μM respectively. Spectra are unchanged upon standing from ca. 0.2-24 hr.

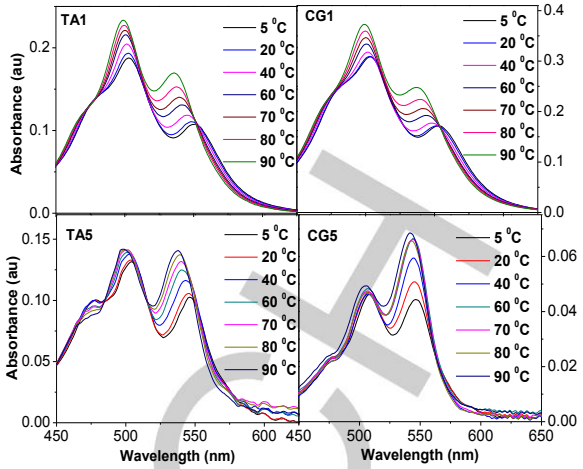

Figure 6. The long-wavelength region of the UV-visible spectra of conjugates **TA-1, 5** and **CG-1, 5** in aqueous buffer at temperatures between 5 and 90 oC. Approximate concentrations for **TA1**: 5.2 μM, **TA5**: 3.6 μM, **CG1**: 8.4 μM, **CG5**: 2.1 μM..

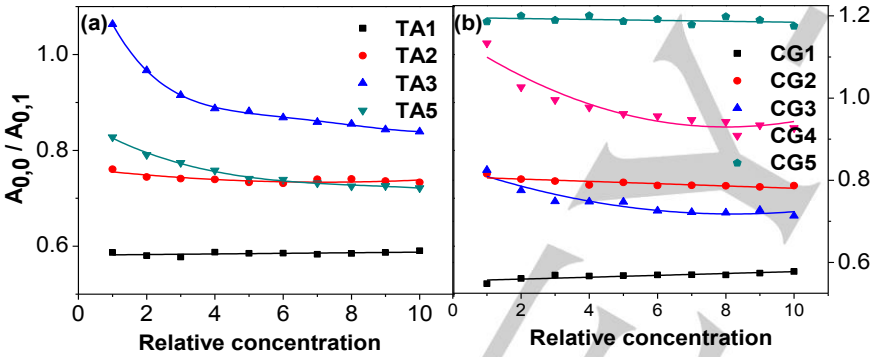

Figure 5. Concentration dependence of the 0,0/0,1 vibrionic band intensity ratios for (a) **TA1-5** and (b) **CG1-5**. Maximum concentrations: **TA1**: 7.4 μM, **TA2**: 5.1 μM, **TA3**: 4.5 μM, **TA5**: 5.9 μM, **CG1**: 6.5 μM, **CG2**: 6.6 μM, **CG3**: 6.4 μM, **CG5**: 2.2 μM.

reduced PDI-PDI overlap. Examples of PDI dimers with slipped-stack geometries having vibrionic band intensity ratios similar to those of **TA2** and **CG2** have previously been reported.[23]

The PDI 0,0/0,1 vibrionic band intensity ratios for **TA3** decrease with increasing concentration (Figure 5), unlike the ratios for **TA1-2** and **CG1-2** which are independent of concentration. The higher values of the vibrionic band intensity ratios for **TA3** vs. **TA1-2** plausibly reflect the increased solubility of the conjugates as the length of their hydrophilic oligo tails increases. Increasing concentration results in a linear increase in 250 nm absorbance of the **TA3** oligo tail (Figure S14, SI), indicating that there is no appreciable duplex formation at high concentration.

The temperature-dependence of the long-wavelength region of the UV-visible spectra of the conjugates in aqueous buffer are shown in Figure 6 and S15 SI and plots of the temperature dependence of the 0,0/0,1 vibrionic band intensity ratios are shown in Figure 7. The ratio for **TA1** increases upon heating from 0.55 at 5 °C to 0.73 at 90 °C. An even smaller increase is observed for **CG1**. Both the initial and final values are higher for **TA2**, **TA3**, and **CG2**. In the case of **TA3** the changes in band shape which occur upon heating are fully reversible upon cooling to 5 °C (Figure S16). The thermal profiles for **TA1-3** and **CG1-2** display a flat region at lower temperatures and a continuous increase at higher temperatures (Figure 7). Increasing the temperature affects a gradual increase in the PDI 0,0/0,1 vibrionic band intensity ratio beginning around room temperature (Figure 7). The sigmoid temperature dependence for **TA3** is consistent with isodesmic aggregation.[24] Plots of α, the degree of aggregation, and <N>, the average number of PDIs in an aggregate vs. temperature for **TA3** are shown in Figure S17, SI. Values of α and <N> are 0.90 and 3 ± 1 at 20 °C and $K = 4.8 \times 10^5$ L/mol. Whereas complete melting profiles are not available for the conjugates with shorter oligo tails, the higher degree of aggregation for **TA1-2** ($\alpha \geq 0.95$, Figure S17b, SI) indicates that they have larger association constants ($K > 1 \times 10^6$ L/mol) than does **TA3**. The CD spectrum of **TA3** also shows a continuous decrease in the intensity of its bissignate long-wavelength bands with increasing temperature (Figure S11, SI).

The temperature dependencies of the absorbance of the base-pair maxima near 250 nm for **TA1** and **CG1** are too small to be determined accurately. For **TA2**, **TA3**, and **CG2**, the changes in 250 nm absorbance parallel those for the 0,0/0,1 vibrionic band intensity ratios (Figure S18a,b, SI). The PDI

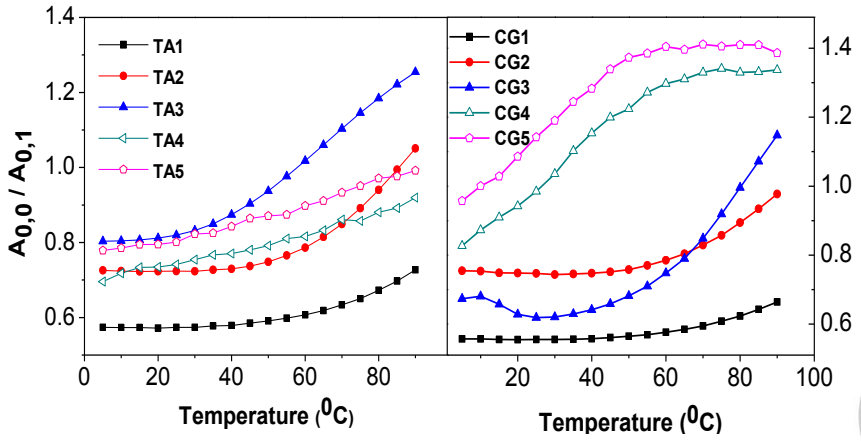

Figure 7. Temperature dependence of the ratio of 550/505 nm vibronic band intensities for conjugates **TA1-5** and **GC1-5.**

0,0/0,1 vibronic band intensity ratios are also independent of temperature below 40-50 ºC and increase gradually at higher temperature (Figure 7). The 255 nm absorbance for **TA2** increases slightly with increasing temperature, but does not display a melting transition (Figure S18a, SI).

The PDI 0,0/0,1 vibronic band intensity ratio for **TA1** is essentially independent of NaCl concentration; whereas the ratios for **TA2-3** decrease slightly upon addition of salt (Figure S19a, SI). We previously reported that PDI linked hairpins[16] and dumbbells[17] having eight or more base pairs exist as monomers in aqueous solution in the absence of added salt, but undergo essentially quantitative dimerization and polymerization, respectively, upon addition of 0.1 M NaCl (Scheme 1). Salt-induced PDI association was attributed to "salting out" (hydrostriction) of the large hydrophobic PDI chromophores. Hence the **TA1-2** conjugates presumably are extensively associated prior to addition of NaCl so that little further association occurs upon addition of salt.

The UV-vis spectra of conjugates **TA1,3,5** and **CG1,3,5** in the base-pair denaturing solvent dimethyl sulfoxide (DMSO)[25] without aqueous co-solvent are shown in Figure S20, SI. The 0,0/0,1 vibronic band intensity ratio for **TA3** is ca. 1.5, indicative of a high monomer/aggregate ratio. This ratio decreases with increasing water content in mixed solvent (data not shown). Lower values of the band intensity ratio are observed for **TA1** (1.14) and **CG1** (1.03), indicative of partial PDI stacking even in 100% DMSO.

The fluorescence spectra of several of the conjugates in buffer are shown in Figure S21, SI. Both **CG1** and **TA3** display very weak structured emission characteristic of PDI conjugate monomers.[16] Evidently, the PDI-stacked aggregates which are the dominant species present in solution for these conjugates are even more weakly fluorescent than are the PDI monomers.

In summary, conjugates **TA1-3** and **CG1-2** form aggregates having stacked PDI head groups and solvated oligo tails in aqueous solution at room temperature. Stacking of **TA3** occurs via an isodesmic mechanism with an average stacking number of 3 molecules per stack at room temperature (Scheme 2a). There is no evidence for the base pairing between the short *N*-oligo tails of these conjugates in aqueous solution either in the presence or absence of 0.1 M NaCl. In the case of **TA1** and **TA3** the aggregates are chiral, as evidenced by their bissignate CD spectra, whereas the aggregates of **TA2** are achiral. The PDI stacked aggregates of **CG1** have very weak monomer and excimer fluorescence, as is the case for **TA3** (Figure S21, SI). Thus neither the length nor the strength of A-T vs. C-G base pairing influences the aggregation of these conjugates which is determined by PDI stacking and by solubility. Cryo-TEM imaging reveals the formation of fibres containing larger numbers of stacked PDI head groups (ca. 35-45 conjugates, Scheme 2a). The larger aggregate size in the cryo-TEM images vs. the ones determined by the thermodynamic studies may reflect higher concentrations used for cryo-TEM imaging and a bias in the cryo-TEM image analysis for larger aggregate sizes (shorter fibres are more difficult to identify).

Structures of Conjugates TA4-5. The cryo-TEM images of **TA4-5** (Figure 2b,c) show the formation of linear fibres with diameters similar to those for **TA1-3** (Table S3, SI). In addition, the images of **TA4-5** display parallel structures with high contrast domains. Here, fibre bundles could be formed by cooperative anti-parallel hydrogen bonding between the ends of the oligo tails extending from each of the fibres, as shown in Scheme 3a. In the case of **TA5** the most notable features are parallel high-contrast structures tens to hundreds of nm long having a thickness of 1.3±0.2 nm enclosing a light contrast domain of 1.5 nm. These imaged structures are consistent with the formation of bilayers formed by hydrophobic association of the *N*-alkyl groups from each layer (Scheme 3b).[26] Expectedly, only a relatively small number of cross-sections is observed, since the large bilayer structures tend to orient perpendicularly to the optical axis due to the shear forces induced during sample preparation.

Further evidence for the role of base pairing in the formation of the structures of **TA4-5** is provided by the short-wavelength regions of their CD spectra (Figure 3 and S10, SI) which resemble that of duplex $(TA)_5{\cdot}(TA)_5$ (Figure S12, SI). The long-

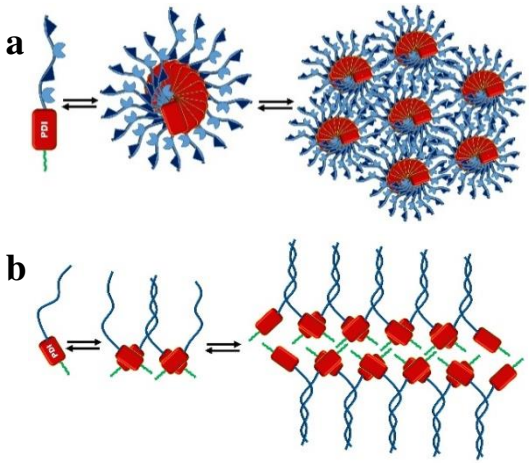

Scheme 3. Schematic for (a) formation of single fibres and bundles of fibres from **TA4** and (b) formation of growing single sheets of side-by-side anti-dimers further assembled into bilayer structures of **TA5**. The bilayer structure is stabilized by PDI π-stacking, hydrophobic alkane interactions, and oligonucleotide parallel duplex formation.

wavelength regions of the CD spectra of **TA4-5** display negative bands attributed to induced CD of the PDI chromophores. The absence of a Cotton effect indicates that the PDI's do not form regular helical stacks similar to those formed by **TA1,3**. The PDI 0,0/0,1 vibronic band intensity ratio for **TA5** decreases with increasing concentration (Figure 5a) and a plot of the 250 nm absorbance vs. concentration displays downward curvature (Figure S14, SI), showing that PDI stacking and base pairing increase with increasing concentration. Both the PDI 0,0/0,1 vibronic band intensity ratios and the 250 nm absorbance for **TA4-5** increase only slightly with increasing temperature (Figure 7 and S17a, SI) showing that their aggregates are more stable than the π-stacked aggregates of **TA1-3**, presumably as a consequence of the combination of π-stacking and hydrogen bonding. **TA5** also remains partially stacked in DMSO, unlike **TA3** which is completely disaggregated in this solvent (Figure S20, SI). This indicates synergy between hydrophobic/stacking induced by PDI groups and base-pairing interactions of the oligonucleotides. Added salt results in a decrease in both the PDI 0,0/0,1 vibronic band intensity ratio and the 250 nm absorbance for **TA4-5** (Figure S19a,c), indicative of increases in both π-stacking and hydrogen bonding.

In summary, the optical spectra of **TA4-5** in aqueous solution are consistent with the formation of stacks of PDI groups which are further stabilized by hydrogen bonding between the oligo tails on different stacks (Scheme 3). Spectroscopic estimation of the degree of aggregation and the average aggregate size is hampered by the occurrence of both π-stacking and hydrogen bonding, which results in greater stability toward thermal dissociation than observed for **TA3** (Figure 7). We note that the duplex formed by the self-complementary sequence $(TA)_5$ is not stable in the absence of added salt; however both **TA4** and **TA5** form duplexes in the absence of salt as a consequence of cooperative PDI-PDI hydrophobic interactions and duplex formation between oligo tails in these conjugates.

Structures of Conjugates CG3-5. The cryo-TEM images of **CG3** are similar to those of **CG1** but the average fibre length is shorter than that of **CG2** (Table S4, SI). The single fibres of **CG3** are assigned to PDI π-stacked aggregates similar to those formed by **CG1-2**. Some areas of the cryo-TEM image of **CG3** contained disc-like aggregates consisting of packed fibres oriented parallel to the optical axis (Figure S8, SI). The cryo-TEM images of **CG4-5** show the formation of fibrous aggregates (Figure 2d,e and Figure S9, SI). The images for **CG5** are of sufficiently high quality to permit resolution of ordered arrays

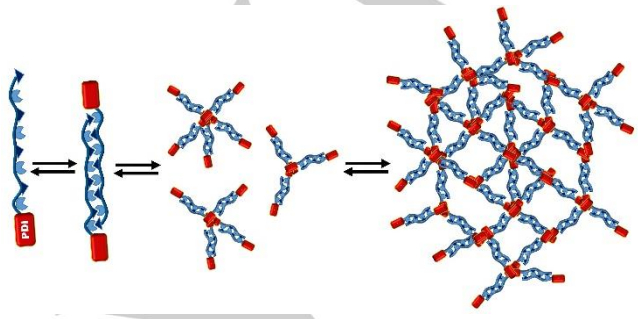

Scheme 4. Schematicfor formation of base-paired duplexes from PDI conjugates with long $(CG)_n$ tails (n = 3-5) and assembly of the duplexes into PDI π-stacked arrays. *N*-Alkyl groups omitted for clarity.

constructed from high-contrast point-like structures, which are assigned to the PDI stack termini packed mainly parallel to the optical axis in ordered arrays with a radial distribution function of 5.2 ± 0.2 nm.

The PDI 0,0/0,1 vibronic band intensity ratio for **CG3** decreases with increasing concentration (Figure 5b), indicative of increased PDI π-stacking, but increases with increasing temperature above 50 °C (Figure 7b), indicative of PDI unstacking. The plot of 250 nm absorbance vs. concentration for **CG3** displays downward curvature (Figure S14, SI), indicative of increased base pairing and the plot of 250 nm absorbance vs. temperature (Figure S18b, SI) has a sharp melting transition at ca. 12 °C. Further evidence for an abrupt change in structure immediately below room temperature is provided by the CD spectra shown in Figure S11 (SI), which displays a marked decrease in the strength of the long-wavelength Cotton effect, accompanied by an increase in strength of the 210 nm band characteristic of base pairing (Figure S12, SI). Added salt has little effect on the PDI 0,0/0,1 vibronic band intensity ratio for **CG3** at room temperature (Figure S19, SI). Evidently, this conjugate has π-stacked structures at room temperature and thus the addition of salt does not appreciably change the extent of stacking.

In summary, **CG3** forms π-stacked aggregates similar to those formed by CG1-2 at room temperature in solution. Below room temperature these aggregates are formed in equilibrium with anti-parallel duplexes in which the PDI head groups can serve as duplex capping groups (Scheme 4), as proposed by Baumstark and Wagenknecht for PDI conjugates with longer oligo tails having non-repeating base sequences.[10] The π-stacked aggregates are the precursors of the single fibres observed in the cryo-TEM images. The ordered aggregate arrays are discussed further with CG4-5.

CG4-5 display short wavelength CD bands (Figure 3d and S10, SI), similar to those of the duplexes $(CG)_3$•$(CG)_3$ and $(CG)_5$•$(CG)_5$ (Figure S12, SI), consistent with the formation anti-parallel duplexes at room temperature. The CD spectra of **CG4-5** show only induced CD bands for PDI, similar to those for hairpin **H8** and dumbbell **D8** which exist as monomers in the absence of added salt (Scheme 1).[16, 17] The PDI 0,0/0,1 vibronic band intensity ratios for **CG4** decrease as its concentration increases, indicative of increased π-stacking; however no such increase occurs for **GC5** (Figure 5b). A plot of the 260 nm absorbance vs. concentration for **CG5** displays slight downward curvature (Figure S14, SI), consistent with an increase in base pair formation. Upon heating the position and band shapes of the 0,0 and 0,1 PDI bands of **CG4-5** undergo little change (Figure 6, S15 and Table S3). The PDI 0,0/0,1 vibronic band intensity ratios for **CG4-5** display similar temperature dependence (Figure 7b) increasing with a linear slope until attaining a value approaching 1.4, characteristic of the conjugate monomers. This temperature dependence is unique to **CG4-5** of the PDI conjugates investigated and is attributed to melting of end-capped duplexes, which exist as monomers above 50 °C in the absence of added salt.

Added salt results in a decrease in the PDI 0,0/0,1 vibronic band intensity ratios for **CG4-5**, the effect being larger for **CG5**, which has the larger band intensity ratio in the absence of salt (Figure S19, SI). **CG2-5** have similar values of the PDI 0,0/0,1 vibronic band intensity ratio in the presence of 100 mM NaCl. The effect of added salt might be attributed to either an

increase in π-stacking of the PDI head groups or increased base pairing of the oligo tails accompanied by oligomerization of the resulting end-capped duplexes. In the absence of added salt, neither the end capped duplexes nor PDI-linked dumbbells undergo appreciable oligomerization,[17] as evidenced by the high PDI 0,0/0,1 vibrionic band intensity ratio and absence of excimer fluorescence (Figure S21, SI). Added salt does result in a reduction in the 260 nm base pair absorbance of **GC3-5** (Figure S19, SI) attributed to an increase in base pairing. The effect is greatest for **GC3** and least for **GC5** reflecting the strength of the duplexes formed by the longer oligo tails.

The basic structural unit for conjugates **CG4-5** in dilute solution at room temperature is the end-capped duplex (Scheme 4), which undergoes base-pair melting to yield the PDI conjugate monomer upon heating (Figure 7b). The duplexes can further assemble into PDI stacks (Scheme 4), whose concentration increases as the oligo tail becomes shorter (Figure 5b) or the conjugate or salt concentration increases. These PDI stacks can further assemble into arrays of stacked PDI head groups connected by 10-bp duplexes. A 10-bp duplex plus the two propylphosphate linkers would have an estimated length of ≥ 4.5 Å, in good agreement with the inter-fibre distance derived from RDF analysis of **CG5** (Figure 2f).

Conclusions

The interplay of hydrophobic π-stacking of PDI head groups and base pairing of oligo tails in the PDI-oligonucleotide conjugates in Chart 1 in aqueous solution results in a diverse structural space that includes fibres and more complex aggregates (Scheme 3 and 4 and Table S3, SI). The stability of the π-stacked PDI assemblies of **TA1-3** and **CG1-3** are similar, indicating that the choice of structural motif is dependent mainly upon the length of the oligo tail and the strength of its base pairing. Conjugates with short oligo tails (**TA1-3** and **CG1-2**) form only π-stacked PDI assemblies in solution. The PDI π-stacked assemblies of **TA4-5** are further stabilized by intrastrand bonding between their oligo tails. Dominated by PDI stacking, assemblies of **TA1-3** form fibres of variable lengths. **TA4-5** form bilayer structures as a result of both stacking and oligonucleotide base pairing (Scheme 3). The oligo tails of **CG4-5** form end-capped duplexes which can further assemble into large PDI-π-stacked arrays (Scheme 4).

Previous studies of the self-assembly of PDI-DNA conjugates have revealed a single dominant mode of assembly. For example PDI-linked hairpins yield only head-to-head dimers[16] and PDI linked dumbbells and doubly-end-capped duplexes or dumbbells yield only linear oligomers assembled with simple PDI-PDI hydrophobic association (Scheme 1).[10, 17] The PDI-conjugates **TA1-3** and **CG1-3** also have PDI π-stacking as their dominant mode of association at room temperature in aqueous solution; however the length of the oligo tail serves to modulate their solubility. The conjugates **TA4-5** and **CG4-5** can undergo self-assembly by means of base pair formation as well as π-stacking/hydrophobic interactions induced by PDI groups, thereby expanding the diversity of their structural space. In the case of **TA4-5** π-stacking remains the primary mode of self-assembly in solution, whereas in the case of **CG4-5** base pairing is the primary mode of self-assembly, underscoring a potential of precise oligo design to impact self-assembly and achieve novel complex structural motifs. Thus, interplay of interactions induced by a large aromatic moiety and a short oligonucleotide pendant represents a versatile addition to the tool box for control over self-assembly and achieving novel structural motifs.

Experimental Section

DNA-Conjugates. The N-alkylperylenediimide derivative was prepared by a modification of the procedure reported by Wagner and Wagenknecht.[20] The PDI-conjugates shown in Chart 1 were prepared by methods reported previously.[27] The conjugates were purified by reverse phase HPLC (Figure S1 SI) and characterized by their MALDI-TOF mass spectra (m/z values reported in Table S1, SI). Circular dichroism (CD) spectra were recorded on Jasco J-815 CD spectrometer. All spectroscopic studies were performed in 10 mM phosphate buffer (pH 7.2) without added salt, unless otherwise mentioned. Solutions were prepared by addition of small aliquots of a concentrated solution of the conjugate to the buffer. UV and CD spectra were recorded within 10-20 min after preparation of the samples. For several of the samples, spectra were recorded again and did not change after 1 hr time increments as long as 24 hr. Concentrations of the conjugate reported in the figure captions or coordinates were determined relative to the highest concentration at room temperature, assuming high values of α under these conditions (Figure S17). The absorption coefficient of 36,400 $M^{-1}cm^{-1}$ at the absorption maximum reported by Rehm et al. or a water-soluble PDI derivative was employed.[5] Solutions in DMSO were prepared without aqueous co-solvent.

MD simulations. *Parameterization.* **TA1** and **TA2**, including explicit water and ions, were simulated with the amber force field.[28] Charges for the PDI rSIdue were derived from the B3LYP/6-31G* optimized geometry as determined using Gaussian 09.[29] The electrostatic potential around the optimized geometry was computed using the HF/6-31G* level of theory and fit to atomic charges using the restrained electrostatic potential module in amber.[30] The remaining parameters for the PDI rSIdue (bonds, angles, dihedral and Lennard-Jones parameters) were taken from identical atom types in the generalized amber force-field (gaff). Likewise, parameters to describe the connection of PDI and nucleotides were also taken from gaff.[28]

All-atom Molecular Dynamics. The parameterized **TA1** structures were subjected to 150 ns all atom MD simulation from six different starting configurations each in water with only neutralizing salt ions present. **TA2** was run for 75 ns from four starting configurations. Each of the starting configurations had a TIP3P water box added using tLeap**1**, extending 12 Å in all directions. Sodium ions were added only to neutralize the nucleotides, such that each system had an overall charge of zero. Each simulation was heated to 298 K and the pressure was held constant at 1 bar. NAMD2.1[31] was used for simulation, implementing the AMBER force fields.[28] VMD 1.9.2 was used to visualize trajectories of each simulation.[32] The different starting configurations were intended to obtain an initial understanding of PDI dimer structures and their formation. Trajectories of these PDI dimers were used to extract starting coordinates for Umbrella sampling, whereby PDI dimer structures whose angle between major axes fell in the range of

0° to 180° were saved. Presumably, the angle of these axes would have a large influence on the thermodynamic stability of the dimer.

Umbrella Sampling. A logical procedure to probe the effect of change in the major axes angle was to harmonically constrain the PDI dimer in these 18 sequential dihedral "windows", from 0° to 180°. The dihedral was defined as shown in Figure S4, SI, between each corresponding PDI nitrogen and the center of mass of that PDI's nitrogens. This method was achieved using the Collective Variables module of NAMD.**5**A. 0.1 kcal/mol was all that was necessary to constrain these dihedral states into their dSIred equilibrium value of 0° to 180° for 40 ns. The dihedral angle each PDI dimer occupied during the final 15 ns of simulation was compared to its respective equilibrium dihedral and the effect of the biasing force was removed using the Weighted Histogram Analysis Method (WHAM).[33] The result is a potential of mean force along the dihedral coordinate. For the sake of visual clarity, the 0° to 180° data was mirrored to represent a full 0° to 360° rotation.

Cryo-transmission electron microscopy (cryo-TEM). Imaging was performed using a Tecnai F20 transmission electron microscope operating at 200 kV, and using a Gatan 626 cooling holder and transfer station with a Gatan US4000 CCD digital camera, or a Tecnai T12 transmission electron microscope operated at 120 kV, using a Gatan 626 cooling holder and transfer station, with a TVIPS F244HD CCD digital camera. *Sample-preparation:* 8 µL of each sample was applied to a 300-mesh copper grid coated with holey carbon (Pacific Grid-Tech supplies). The samples were blotted at 25°C and 95% relative humidity, and plunged into liquid ethane using Leica EM-GP Automatic Grid Plunger. Samples were aged for a minimum of 24 hr at room temperature prior to imaging. Images did not change upon further aging. Radial Distribution Function was calculated by utilizing a macro written for the FIJI software.[34]

Acknowledgements

This research is supported by a grant from the US-Israel Binational Science Foundation (Grant No. 2010114 to FDL and BR). The cryo-TEM studies were conducted at the Irving and Cherna Moskowitz Center for Nano and Bio-Nano Imaging (Weizmann Institute). This work used the Extreme Science and Engineering Discovery Environment (XSEDE), which is supported by National Science Foundation grant number ACI-1053575. MM and KAV were supported by computing time on XSEDE through allocation TG-CHE160008.

Keywords: pi-interaction • aggregation • hydrophobic effect • DNA base pairing • imaging

References

[1] R. Marty, R. Szilluweit, A. Sánchez-Ferrer, S. Bolisetty, J. Adamcik, R. Mezzenga, E.-C. Spitzner, M. Feifer, S. N. Steinmann, C. Corminboeuf, H. Frauenrath, *ACS Nano* **2013**, *7*, 8498.

[2] a) M. R. Wasielewski, *Acc. Chem. Res.* **2009**, *42*, 1910; b) F. Würthner, C. R. Saha-Möller, B. Fimmel, S. Ogi, P. Leowanawat, D. Schmidt, *Chem. Rev.* **2016**, *116*, 962; c) E. Krieg, B. Rybtchinski, *Chem. Eur. J.* **2011**, *17*, 9016.

[3] D. Görl, X. Zhang, F. Würthner, *Angew. Chem. Int. Ed.* **2012**, *51*, 6328.

[4] J. Gershberg, M. Radić Stojković, M. Škugor, S. Tomić, T. H. Rehm, S. Rehm, C. R. Saha-Möller, I. Piantanida, F. Würthner, *Chem. Eur. J.* **2015**, *21*, 7886.

[5] S. Rehm, V. Stepanenko, X. Zhang, T. H. Rehm, F. Würthner, *Chem. Eur. J.* **2010**, *16*, 3372.

[6] G. Echue, G. C. Lloyd-Jones, C. F. J. Faul, *Chem. Eur. J.* **2015**, *21*, 5118.

[7] C. D. Schmidt, C. Böttcher, A. Hirsch, *Eur. J. Org. Chem.* **2009**, *2009*, 5337.

[8] T. Heek, C. Fasting, C. Rest, X. Zhang, F. Würthner, R. Haag, *Chem. Commun.* **2010**, *46*, 1884.

[9] W. Wang, W. Wan, H. H. Zhou, S. Q. Niu, A. D. Q. Li, *J. Am. Chem. Soc.* **2003**, *125*, 5248.

[10] D. Baumstark, H. A. Wagenknecht, *Angew. Chem. Int. Ed.* **2008**, *47*, 2612.

[11] a) F. Menacher, V. Stepanenko, F. Würthner, H.-A. Wagenknecht, *Chem. Eur. J.* **2011**, *17*, 6683; b) C. Stubinitzky, A. Bijeljanin, L. Antusch, D. Ebeling, H. Hölscher, H.-A. Wagenknecht, *Chem. Eur. J.* **2014**, *20*, 12009.

[12] F. Menacher, H.-A. Wagenknecht, *Photochem. Photobiol. Sci.* **2011**, *10*, 1275.

[13] a) D. Baumstark, H. A. Wagenknecht, *Chem. Eur. J.* **2008**, *14*, 6640; b) H. Kashida, H. Asanuma, *Phys. Chem. Chem. Phys.* **2012**, *14*, 7196; c) Y. Zheng, H. Long, G. C. Schatz, F. D. Lewis, *Chem. Commun.* **2005**, 4795.

[14] T. Takada, M. Ido, A. Ashida, M. Nakamura, K. Yamana, *ChemBioChem* **2016**, *17*, 2230.

[15] C. Haas, K. Kraling, M. Cichon, N. Rahe, T. Carell, *Angew. Chem., Int. Ed.* **2004**, *43*, 1842.

[16] M. Hariharan, Y. Zheng, H. Long, T. A. Zeidan, G. C. Schatz, J. Vura-Weis, M. R. Wasielewski, X. B. Zuo, D. M. Tiede, F. D. Lewis, *J. Am. Chem. Soc* **2009**, *131*, 5920.

[17] P. Neelakandan, Z. Pan, M. Hariharan, Y. Zheng, B. Rybtchiski, H. Weissman, F. D. Lewis, *J. Am. Chem. Soc.* **2010**, *132*, 15808.

[18] M. Hariharan, K. Siegmund, Y. Zheng, H. Long, G. C. Schatz, F. D. Lewis, *J. Phys. Chem. C* **2010**, *114*, 20466.

[19] Y.-L. Wu, K. E. Brown, M. R. Wasielewski, *J. Am. Chem. Soc.* **2013**, *135*, 13322.

[20] C. Wagner, H. A. Wagenknecht, *Org. Lett.* **2006**, *8*, 4191.

[21] E. Hädicke, F. Graser, *Acta Cryst. C* **1986**, *42*, 189.

[22] a) V. Dehm, Z. Chen, U. Baumeister, P. Prins, L. D. A. Siebbeles, F. Würthner, *Org. Lett.* **2007**, *9*, 1085 b); P. A. J. De Witte, J. Hernando, E. E. Neuteboom, E. M. H. P. van Dijk, S. C. J. Meskers, R. A. J. Janssen, N. F. van Hulst, R. J. M. Nolte, M. F. García-Parajó, A. E. Rowan, *J. Phys. Chem. B* **2006**, *110*, 7803.

[23] a) P. P. Neelakandan, T. A. Zeidan, M. McCullagh, G. C. Schatz, J. Vura-Weis, C. H. Kim, M. R. Wasielewski, F. D. Lewis, *Chem. Sci.* **2014**, *5*, 973; b) E. A. Margulies, L. E. Shoer, S. W. Eaton, M. R. Wasielewski, *Phys. Chem. Chem. Phys.* **2014**, *16*, 23735.

[24] a) D. H. Zhao, J. S. Moore, *Org. Biomol. Chem.* **2003**, *1*, 3471; b) J. D. Fox, S. J. Rowan, *Macromolecules* **2009**, *42*, 6823; c) T. F. A. De Greef, M. M. J. Smulders, M. Wolffs, A. P. H. J. Schenning, R. P. Sijbesma, E. W. Meijer, *Chem. Rev.* **2009**, *109*, 5687; d) M. M. J. Smulders, M. M. L. Nieuwenhuizen, T. F. A. de Greef, P. van der Schoot, A. P. H. J. Schenning, E. W. Meijer, *Chem. Eur. J.* **2010**, *16*, 362.

[25] G. Bonner, A. M. Klibanov, *Biotech. Bioeng.* **2000**, *68*, 339.

[26] Y. Tidhar, H. Weissman, D. Tworowski, B. Rybtchinski, *Chem. Eur. J.* **2014**, *20*, 10332.

[27] a) T. A. Zeidan, R. Carmieli, R. F. Kelley, T. M. Wilson, F. D. Lewis, M. R. Wasielewski, *J. Am. Chem. Soc.* **2008**, *130*, 13945; b) T. M. Wilson, T. A. Zeidan, M. Hariharan, F. D. Lewis, M. R. Wasielewski, *Angew. Chem., Int. Ed.* **2010**, *49*, 2385.

[28] W. D. Cornell, P. Cieplak, C. I. Bayly, I. R. Gould, K. M. Merz, D. M. Ferguson, D. C. Spellmeyer, T. Fox, J. W. Caldwell, P. A. Kollman, *J. Am. Chem. Soc.* **1995**, *117*, 5179.

[29] G. W. T. M. J. Frisch, H. B. Schlegel, G. E. Scuseria, M. A. Robb, J. R. Cheeseman, G. Scalmani, V. Barone, G. A. Petersson, H. Nakatsuji, X. Li, M. Caricato, A. Marenich, J. Bloino, B. G. Janesko, R. Gomperts, B. Mennucci, H. P. Hratchian, J. V. Ortiz, A. F. Izmaylov, J. L. Sonnenberg, D. Williams-Young, F. Ding, F. Lipparini, F. Egidi, J. Goings, B. Peng, A. Petrone, T. Henderson, D. Ranasinghe, V. G. Zakrzewski, J. Gao, N. Rega, G. Zheng, W. Liang, M. Hada, M. Ehara, K. Toyota, R. Fukuda, J. Hasegawa, M. Ishida, T. Nakajima, Y. Honda, O. Kitao, H. Nakai, T. Vreven, K. Throssell, J. A. Montgomery, Jr., J. E. Peralta, F. Ogliaro, M. Bearpark, J. J. Heyd, E. Brothers, K. N. Kudin, V. N. Staroverov, T. Keith, R. Kobayashi, J. Normand, K. Raghavachari, A. Rendell, J. C. Burant, S. S. Iyengar, J. Tomasi, M. Cossi, J. M. Millam, M. Klene, C. Adamo, R. Cammi, J. W. Ochterski, R. L. Martin, K. Morokuma, O. Farkas, J. B. Foresman, and D. J. Fox, Gaussian, INC, Wallingford CT, **2009**.

[30] P. C. C. I. Bayly, W. D. Cornell, P. A. Kollman, *J. Phys. Chem.* **1993**, *97*, 10269; V. B. D. A. Case, J.T. Berryman, R.M. Betz, Q. Cai, D.S. Cerutti, T.E. Cheatham, III, T.A. Darden, R.E. Duke, H. Gohlke, A.W. Goetz, S. Gusarov, N. Homeyer, P. Janowski, J. Kaus, I. Kolossváry, A. Kovalenko, T.S. Lee, S. LeGrand, T. Luchko, R. Luo, B. Madej, K.M. Merz, F. Paesani, D.R. Roe, A. Roitberg, C. Sagui, R. Salomon-Ferrer, G. Seabra, C.L. Simmerling, W. Smith, J. Swails, R.C. Walker, J. Wang, R.M. Wolf, X. Wu and P.A. Kollman University of California San Francisco, **2014**.

[31] J. C. Phillips, R. Braun, W. Wang, J. Gumbart, E. Tajkhorshid, E. Villa, C. Chipot, R. D. Skeel, L. Kalé, K. Schulten, *J. Comput. Chem.* **2005**, *26*, 1781.

[32] W. Humphrey, A. Dalke, K. Schulten, *J. Mol. Graphics* **1996**, *14*, 33.

[33] A. Grossfield, WHAM: the weighted histogram analysis method. Version 2.0.9.

[34] J. Schindelin, I. Arganda-Carreras, E. Frise, V. Kaynig, M. Longair, T. Pietzsch, S. Preibisch, C. Rueden, S. Saalfeld, B. Schmid, J.-Y. Tinevez, D. J. White, V. Hartenstein, K. Eliceiri, P. Tomancak, A. Cardona, *Nat. Meth.* **2012**, *9*, 676;.

10.1002/chem.201700752

WILEY-VCH

Entry for the Table of Contents (Please choose one layout)

Layout 1:

FULL PAPER

Heads or Tails? Assembly of perylenediimide-single strand DNA conjugates can be directed to different structural space by the interplay between π-stacking and base pairing. When the oligo tails are short, stacking of the PDI heads to form fibres wins. When $(AT)_n$ tails are long cross-linking of the fibres occurs. When $(GC)_n$ tails are long, base pairing dominates leading to formation of bilayers and ordered arrays.

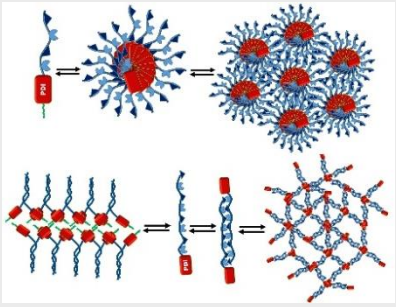

Ashutosh Kumar Mishra, Haim Weissman, Elisha Krieg, Kevin A. Votaw, Martin McCullagh, Boris Rybtchinski, and Frederick D Lewis**

Page No. – Page No.

Self-assembly of perylenediimide-single strand DNA conjugates: Employing hydrophobic interactions and DNA base pairing to create a diverse structural space

Layout 2:

FULL PAPER

((Insert TOC Graphic here; max. width: 11.5 cm; max. height: 2.5 cm))

*Author(s), Corresponding Author(s)**

Page No. – Page No.

Title

Text for Table of Contents